RSC Advances

PAPER

View Article Online
View Journal | View Issue

Cite this: *RSC Adv.*, 2022, **12**, 23584

2D TiVCT$_x$ layered nanosheets grown on nickel foam as highly efficient electrocatalysts for the hydrogen evolution reaction

Yi Wen, Junsheng Yang,* Haoran Zou, Yiquan Fan, Jie Li, Yijian Kuang, Wenkang Liu, Kaisong Zhang and Lieqiang Xiong

Exploring highly efficient and durable catalysts for the hydrogen evolution reaction (HER) is crucial for the hydrogen economy and environmental protection issues. Numerous studies have now found that transition metal carbide MXenes are ideal candidates as catalysts for the hydrogen evolution reaction. However, MXenes are inclined to easily undergo lamellar structure agglomeration and stacking, which impedes their further applications. Besides, most of the extant research has focused on single transition metal carbides, and the investigation of double transition metal carbide MXenes is rather rare. In this research work, a three-dimensional (3D) TiVCT$_x$-based conductive electrode was constructed by depositing 2D TiVCT$_x$ nanosheets on 3D network structured nickel foam (NF) to synthesize a hybrid electrode material (abbreviated as TiVCT$_x$@NF). TiVCT$_x$@NF exhibits efficient electrochemical properties with a low overpotential of 151 mV at 10 mA cm^{-2} and a small Tafel slope of 116 mV dec^{-1}. Benefitting from the open layer structure and strong interfacial coupling effect, compared to the pristine structure, the resulting TiVCT$_x$@NF has greatly increased active sites for the hydrogen evolution reaction (HER) and encounters less resistance for charge transfer. In addition, TiVCT$_x$@NF exhibits better stability in long-term acidic electrolytes. This work provides a tactic to prepare three-dimensional network electrode materials and broadens the application of single transition metal carbide MXenes as water splitting electrodes in the HER, which is beneficial to the application of noble metal-free electrocatalysts.

Received 20th June 2022
Accepted 5th August 2022

DOI: 10.1039/d2ra03791b

rsc.li/rsc-advances

1. Introduction

In recent years, due to the combustion and emission of a variety of chemical fuels, energy shortage and environmental pollution have become global problems. The development of various new and renewable energy sources is an important issue at present. As a secondary energy source, hydrogen energy is clean, efficient, and can be easily stored and transported, and is thus regarded as an ideal energy carrier.[1,2] Water splitting is one of the most promising technologies for industrial hydrogen production.[3] The best electrocatalysts for the HER are platinum electrodes or noble metals; however, due to the rising price of precious metals, the improvement of the catalytic activity and cost-effectiveness of existing metal hydrogen evolution electrodes has become a primary issue for manufacturers.[4,5]

MXenes are two-dimensional transition metal compounds, which can be expressed as $M_{n+1}X_nT_x$ (where M represents a transition metal element, X stands for C or N, and T represents –OH, –F and other functional groups). Many studies[6–9] have shown that MXenes are excellent materials for water electrolysis due to their high specific surface area, good electrical conductivity and stability, which has aroused the extensive interest of scholars. Tang *et al.*[10] proposed that due to the features of the MXene Ti_3C_2 such as its large surface area, excellent conductivity and adjustable terminations, it can be applied in the hydrogen evolution reaction (HER). Huang *et al.*[11] prepared MoS_2/Ti_3C_2 composite heterostructures by the hydrothermal method. When used as a HER electrocatalyst, MoS_2/Ti_3C_2 exhibits excellent electrochemical activity with a low overpotential of ~280 mV at 10 mA cm^{-2}. Compared to MoS_2 nanosheets, the catalytic current density induced by MoS_2/Ti_3C_2 at an overpotential of ~400 mV is more than 6.2 times that of the MoS_2 nanosheets. Le *et al.*[12] used ammonia heat treatment to enhance the hydrogen evolution catalysis of $Ti_3C_2T_x$ MXenes by modification with a nitrogen heteroatom. As shown in the experimental results, compared to the $Ti_3C_2T_x$ MXene, the nitrogen-doped $Ti_3C_2T_x$ annealed at 600 °C exhibited superior HER electrocatalytic performance with an overpotential as low as 198 mV at 10 mA cm^{-2} and a much smaller Tafel slope of 92 mV dec^{-1}. Liu *et al.*[13] mixed $H_8MoN_2S_4$ and $Ti_3C_2T_x$ to prepare $MoS_2/Ti_3C_2T_x$ layered nanomaterials. The active sites of the two-

School of Mechanical Engineering, Wuhan Polytechnic University, Wuhan, 430023, Hubei, China. E-mail: yangjunsheng2008@163.com; Fax: +86-027-85617871

dimensional nanomaterials are greatly increased, the exchange current density is more than 25 times that of MoS_2, and the electrochemical performance is significantly improved.

With the deepening of research, scholars have tried to introduce transition metal elements into MXenes to obtain different electrochemical properties. According to a previous study,[14] compared to Ti_3C_2, the $TiVCT_x$ MXene has some unique electrochemical properties due to the addition of the transition metal element V. Yazdanparast *et al.*[15] successfully obtained MXene thin films of $TiVCT_x$ by etching and layering. The obtained $TiVCT_x$ nanosheets possess a large specific surface area and multiple active sites, and the functional group structure on the $TiVCT_x$ MXene has excellent stability. Li *et al.*[16] investigated the electrochemical properties of the $TiVCT_x$ MXene, and the results showed that the $TiVCT_x$ MXene exhibited metallic properties with high electronic conductivity, and its comprehensive electrochemical performance is better than that of the Ti_2C MXene. Li *et al.*[17] prepared $TiVCT_x$ MXenes and investigated their electrochemical properties, and discovered that the performance of the $TiVCT_x$ MXenes did not yield the desired results. They then used *o*-phenylenediamine (*o*-PD) as a metamer for oxidant-free polymerization and mixed it with the prepared $TiVCT_x$ to obtain three-dimensionally stable $TiVCT_x$/poly-*o*-PD hybrids. Electrochemical studies have shown that the $TiVCT_x$/poly-*o*-PD hybrid possessed a high specific surface area, excellent cycling stability, and improved comprehensive electrochemical performance. Nevertheless, there are few reports on the hydrogen evolution performance of the $TiVCT_x$ MXene in the electrolysis of water.

Ni is an abundant transition metal element with the features of low cost and high catalytic activity in hydrogen production by water electrolysis.[18] Previous studies have shown that the hybridization of nickel foam (NF) is beneficial to the improvement of the electrochemical performance of nanomaterials.[19–22] Herein, a new strategy is proposed, and the novel hybrid $TiVCT_x$@nickel foam (NF) is obtained by compounding nickel foam with layered MXene nanosheets. The surface element distribution, morphology and structure of $TiVCT_x$@NF are systematically studied, and the electrochemical hydrogen evolution performance and stability of the hybrid nanomaterials are further investigated.

2. Experimental

2.1 Preparation of TiVAlC powders

In a preliminary work, we have successfully prepared TiVAlC powders using TiH_2 (99.6% pure), V (99.6% pure), Al (99.5% pure) and C (99.8% pure) powders with an atomic ratio of 1 : 1 : 1.3 : 1 by the activation reaction sintering method at a sintering temperature of 1500 °C, and the specific details about the preparation of the MAX TiVAlC are shown in Zou's study.[23] Then, the fabricated TiVAlC powders were broken by a crushing machine (GJ500-1, Hangzhou, China) and sieved through a mesh 325 sieve.

2.2 Preparation of $TiVCT_x$ nanosheets

Layered $TiVCT_x$ was synthesized by liquid etching of the as-prepared TiVAlC powders. The etching was carried out by immersing the TiVAlC powders in a 40% HF solution with a solid-to-liquid ratio of 1 : 20 and stirred at 500 rpm for 48 h at 45 °C. Then, the suspension was centrifuged 7–8 times (3 min at a time) at 3500 rpm to separate the multilayered MXene. The centrifuged suspension supernatant was washed and filtered with distilled water until the pH of the supernatant was equal to ~7. After that, the multilayered $TiVCT_x$ MXene was obtained. The obtained multilayered $TiVCT_x$ was stirred with 25% TMAOH solution for 24 h at room temperature. Then, the mixture was centrifuged at 8500 rpm for 5 min, and the supernatant was collected. The $TiVCT_x$ nanosheets were obtained by washing the supernatant with distilled water until the pH of the supernatant was neutral and filtered. The final $TiVCT_x$ nanosheet powders were dried at 50 °C for 12 h in a vacuum oven (DZF-6020, Shanghai, China).

2.3 Preparation of $TiVCT_x$ nanosheets@NF

After sonication for 1 h, 5 mg of the $TiVCT_x$ nanosheets and 20 μL Nafion solution (5 wt%) were dispersed in a 980 μL deionized water/ethanol mixed solution with a volume ratio of 1 : 1. Then, 5 μL of the mixed solution was evenly added to commercial NF (1 cm × 1 cm). After that, the NF loaded with the catalyst was put into a vacuum sintering furnace and sintered in vacuum at 300 °C for 2 h, and $TiVCT_x$ nanosheets@NF was obtained.

2.4 Characterization

The sample powders were analyzed by X-ray diffraction (XRD, D/MAX-rA) using an X-ray diffractometer equipped with Cu Kα radiation ($\lambda = 1.541$ Å). The morphologies of the samples were characterized by scanning electron microscopy (SEM, JSM-5600LV) and transmission electron microscopy (TEM, F200X). The elemental composition of the samples was characterized by scanning electron microscopy equipped with energy dispersive X-ray spectrometry (EDS). The sample surface was characterized by X-ray photoelectron spectroscopy using Mg Kα as the excitation source.

2.5 Electrocatalytic performance evaluation

All electrochemical measurements were carried out using a typical three-electrode configuration with an electrochemical workstation (CHI660E, Shanghai, China). $TiVCT_x$ nanosheets@NF was used as the working electrode (the loading weight is 0.025 mg cm^{-2}), and an Ag/AgCl electrode and glassy carbon electrode were used as the reference electrode and counter electrode, respectively. The HER testing was performed in 0.5 mol L^{-1} H_2SO_4.

For the HER, the potential calibration of the reversible hydrogen electrode (RHE) was calibrated with respect to the following equation:[24]

$$E(\mathrm{RHE}) = E(\mathrm{Ag/AgCl}) + 0.0591\ \mathrm{pH} + 0.196 \quad (1)$$

Cyclic voltammetry (CV) was used to measure the double-layer capacitance (C_{dl}), which was recorded from −6 to 94 mV *vs.* RHE at scan rates from 20 to 120 mV s^{-1} at an interval of 20 mV s^{-1}. Linear sweep voltammetry (LSV) was performed at a scan rate of 10 mV s^{-1} with 90% IR compensation by sweeping the potential from 0 to −0.6 V *vs.* RHE. Electrochemical impedance spectroscopy (EIS) was performed in a frequency range of 100 kHz to 0.01 Hz at an overpotential of open-circuit potential (OCP). The long-term stability test was performed by successive CV at a scan rate of 100 mV s^{-1} for 1000 cycles. Lastly, chronoamperometric measurements at the requisite overpotential to afford 10 mA cm^{-2} were used to evaluate the long-term durability.

3. Results and discussion

In this study, multi-layered $TiVCT_x$ MXenes with different abundant functional groups were successfully prepared through the etching method of removing Al atoms from TiVAlC powder using HF. Ultrathin nanostructured $TiVCT_x$ was obtained by exfoliation. Next, the $TiVCT_x$ nanosheet powders were loaded on commercial nickel foam (NF), and then placed in a vacuum furnace for annealing at 300 °C for 2 h to obtain $TiVCT_x$@NF hybrids (Fig. 1). Fig. 2(a) shows an SEM image of the etched products. It can be clearly seen that a lamellar morphology appears, and these nanosheets are produced by HF etching away the Al in TiVAlC. In order to acquire the micromorphological and structural information of the $TiVCT_x$ MXene in more detail, Fig. 2(b) shows a TEM image of multilayer $TiVCT_x$ and Fig. 2(c) shows a TEM image of few-layer $TiVCT_x$. The multilayered $TiVCT_x$ nanosheets exhibit clearly visible ripples, indicating the ultrathin feature of the $TiVCT_x$ nanosheets. The multilayered $TiVCT_x$ nanosheets present an unordered vertical arrangement. By calculation, the average nanolayer spacing is 2.2 nm (Fig. 2(d and e)).

Fig. 3(a) shows the XRD patterns of TiVAlC and the $TiVCT_x$ MXene after the HF solution etching. It can be seen that the XRD patterns before and after TiVAlC etching are obviously different, indicating the successful synthesis of the $TiVCT_x$ MXene. After the etching of TiVAlC, the diffraction peak intensity at 40.38° is significantly weakened.

Additionally, in the spectrum of the $TiVCT_x$ MXene, a diffraction peak appears at a small angle of 6.85°, indicating the introduction of other molecules (according to a study by Li *et al.*[17]). Fig. 3(b) shows the surface element distribution of the $TiVCT_x$ MXene. It can be seen that the Ti, V, C, F, and O elements are well and uniformly dispersed on the nanosheet structure. The presence of the element O is due to the intercalation of oxygen-containing groups between the nanosheets.

Fig. 4 shows the micromorphology and the results of the elemental distribution of the $TiVCT_x$@NF hybrid materials. Fig. 4(a) exhibits the microstructure of the porous nickel foam framework. In Fig. 4(b), it can be clearly seen that plenty of white nanoparticles are attached to the surface of the nickel foam after hydrothermal treatment. In Fig. 4(c), it can be obviously seen that $TiVCT_x$@NF is composed of Ni, Ti, O, C, F and V, and the six elements are uniformly distributed, indicating the successful synthesis of $TiVCT_x$@NF.

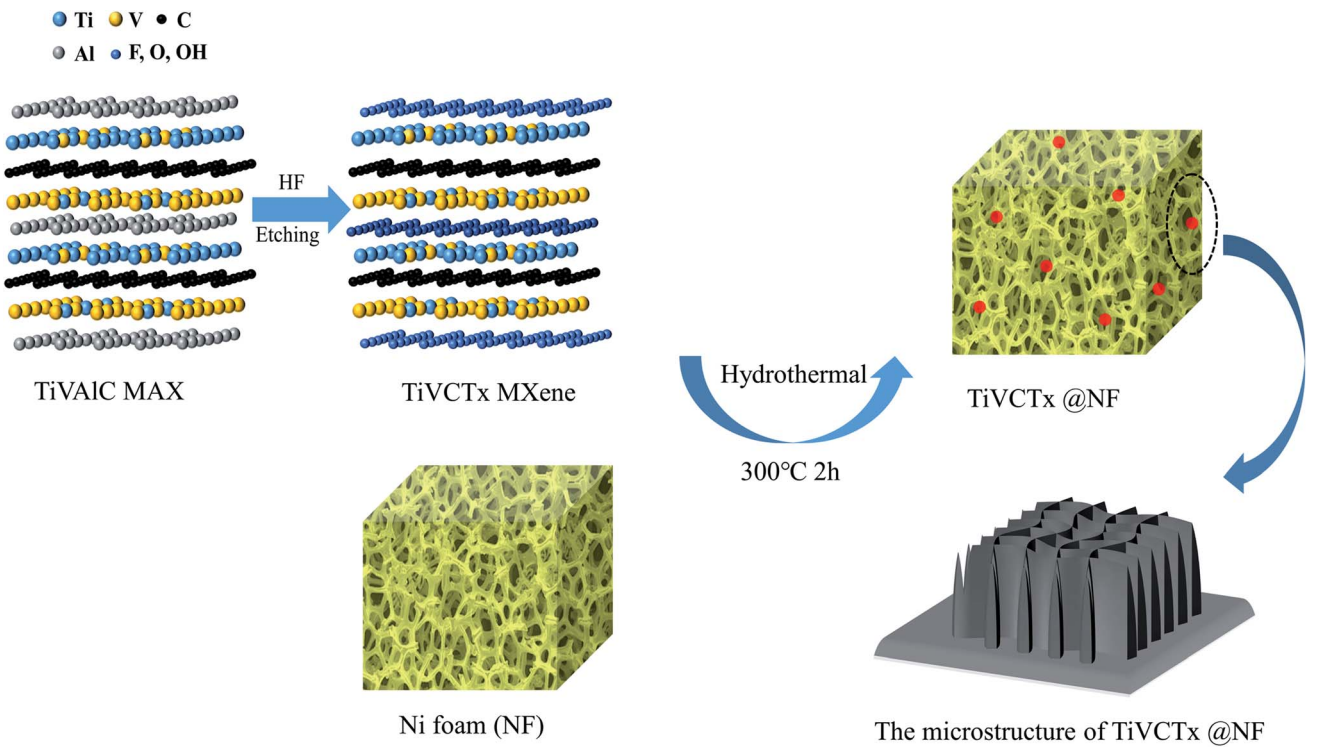

Fig. 1 Schematic illustration of the synthetic process of $TiVCT_x$@NF.

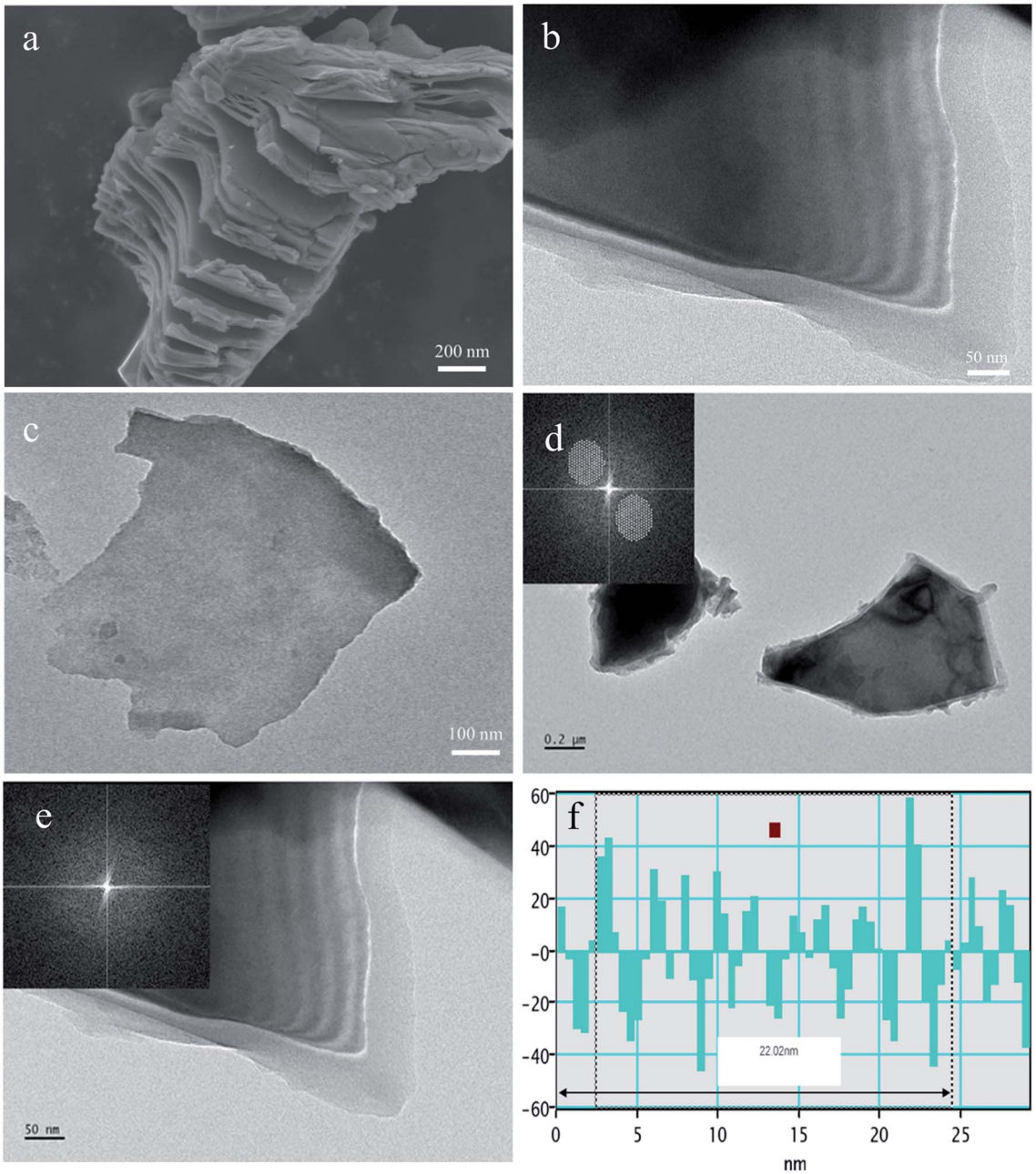

Fig. 2 (a) SEM images of layered TiVCT$_x$. (b and c) TEM images of TiVCT$_x$. (d–f) The interlayer analysis of TiVCT$_x$.

As shown in Fig. 5, XPS was used to analyze the element valence composition of TiVCT$_x$, and PeakFit was used to perform peak processing on the XPS data, and the corresponding characteristic peaks were fixed according to the binding energy. As shown in Fig. 5(b), the spectrum of Ti 2p contains two singlets and one doublet; the peaks at 454.8 eV and 455.36 eV correspond to Ti–C; the peaks at 456.3 eV, 459.2 eV and 464.70 eV correspond to Ti–O; and the peak at 461 eV corresponds to Ti–F. As shown in Fig. 5(c), the binding energy peaks identified for TiVCT$_x$ at 281.6, 282.1, 285.0, 285.3, and 286.3 eV correspond to C=O, C–O, graphitic C–C, C–V, and C–Ti. As shown in Fig. 5(d), the spectrum of F 1s contains two singlets and one doublet. The spectrum is easily fitted by one doublet peak of F–C, which contains two peaks at binding energies of 687.5 eV and 688.5 eV. The peak at 685.4 eV is related to the characteristic F–V, and the peak at 686.4 eV corresponds to C–Ti–F$_x$. The results suggest the embedding of –F in the MXene layered structure. As shown in Fig. 5(e), the spectra of V 2p and O 1s contain V–C, V$_x$O$_y$, V–F, O–Ti, O=V and –OH peaks, indicating the successful etching of Al and the combination of O. In general, it can be clearly seen from the above results that the Al atomic layer is completely etched, and new functional groups (–F, –OH, –O) are introduced. The addition of these functional groups (–F, –OH, –O) may increase the HER catalytic

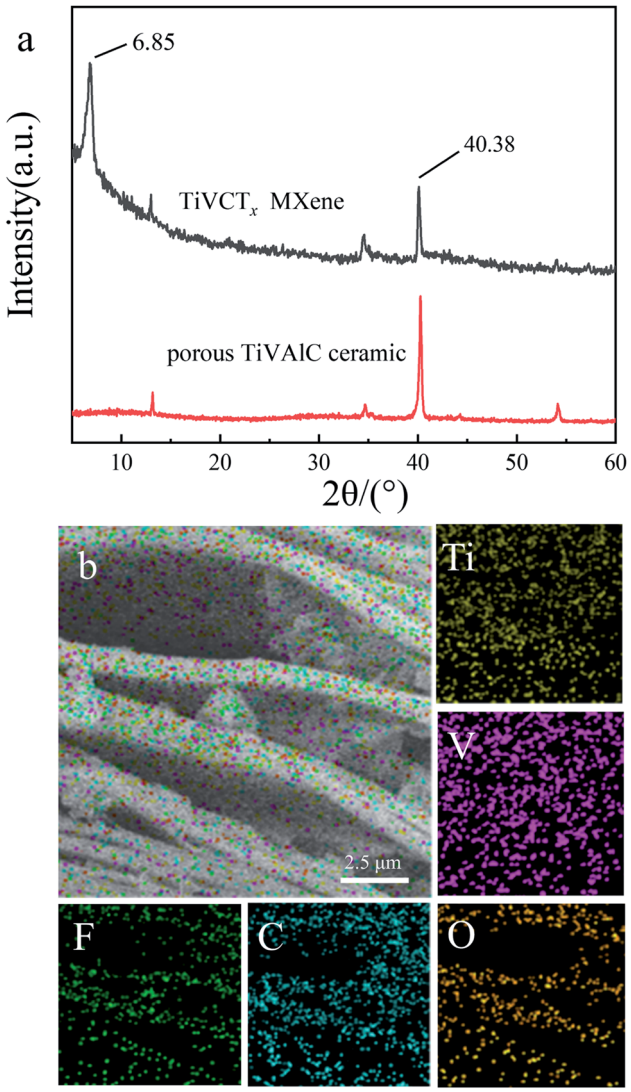

Fig. 3 (a) XRD patterns of the TiVCT$_x$ MXene and TiVAlC powder. (b) Elemental mapping images of layered TiVCT$_x$ nanosheets.

activity of the MXene nanosheets.[25] With the increased adsorption energy of protons, the charge transfer resistance decreases. Due to the surface functional groups, the TiVCT$_x$ nanosheets are negatively charged. Combining the analysis results, the following equations are obtained:

$$2TiVAlC + 6HF \rightarrow 2TiVC + 2AlF_3 + 3H_2\uparrow \quad (2)$$

$$TiVC + 2HF \rightarrow TiVCF_2 + H_2\uparrow \quad (3)$$

$$TiVC + 2H_2O \rightarrow TiVCO_2 + 2H_2\uparrow \quad (4)$$

$$TiVC + 2H_2O \rightarrow TiVC(OH)_2 + H_2\uparrow \quad (5)$$

Electrochemical double-layer capacitance (C_{dl}) is an electrochemical parameter that can evaluate the difference in the electrochemically active surface area of different samples and can be determined by cyclic voltammetry (CV).[26] The number of active sites is one of the important factors determining the HER activity, and the electrochemically active surface area depends on the number of active sites. Fig. 6(a), (c) and (e) present the cyclic voltammetry curves of TiVCT$_x$@NF, TiVCT$_x$ and commercial Pt/C, respectively, measured at scan rates of 20–120 mV s^{-1} with an interval of 20 mV s^{-1}. Fig. 6(b), (d) and (f) present the curves of capacitive current *versus* scan rate for TiVCT$_x$@NF, TiVCT$_x$ and commercial Pt/C at 0.15 V, respectively. It can be seen from the above results that the C_{dl} of TiVCT$_x$@NF is 26.9 mF cm^{-2}, which is much larger than that of TiVCT$_x$ (3.8 mF cm^{-2}), indicating that through the combination with nickel foam, the specific surface area is increased, the active sites are increased, and the hydrogen evolution catalytic performance is enhanced. Besides, the C_{dl} of TiVCT$_x$@NF is close to the C_{dl} of the Pt/C electrode (31.8 mF cm^{-2}).

In order to explain the good electrochemical behavior of the TiVCT$_x$ nanosheets, the relevant tests on their hydrogen evolution performance were carried out. Using a standard three-electrode electrochemical system, the electrochemical activity of TiVCT$_x$ and its hybrid products for the HER was tested in a 0.5 mol L^{-1} H_2SO_4 electrolyte. Besides, the commercial platinum–carbon catalyst (10 wt% Pt/C) with extremely high hydrogen evolution activity and pure nickel foam (NF) were used as references in this test. Fig. 7(a) shows the HER polarization curves of TiVCT$_x$, NF, TiVCT$_x$@NF and commercial platinum–carbon in 0.5 mol L^{-1} H_2SO_4. It can be seen from the figure that the hydrogen evolution overpotential of the TiVCT$_x$ nanosheets obtained after exfoliation at 10 mA cm^{-2} is 583 mV, while the hydrogen evolution overpotential of TiVCT$_x$@NF after modification is 151 mV, which is close to that of the platinum–carbon electrode (33 mV). The hydrogen evolution overpotential of NF at 10 mA cm^{-2} is 261 mV, indicating that the hydrogen evolution catalytic activity of NF is stronger than that of TiVCT$_x$, and the hydrogen evolution catalytic activity is further improved after the combination of TiVCT$_x$ and NF. TiVCT$_x$@NF can be selected as a candidate for excellent hydrogen evolution catalyst materials.

The Tafel slope reveals the rate-determining steps of the hydrogen evolution catalytic reaction. Generally, when the Tafel slope reaches 30 mV, 40 mV or 120 mV, the rate-determining step of the hydrogen evolution catalytic reaction is identified as a Tafel, Heyrovsky or Volmer step, respectively. To understand the kinetics of the hydrogen evolution catalytic reaction of the hybrid TiVCT$_x$@NF in the HER, the Tafel slope was used to reveal its reaction rate-determining steps.[27] Fig. 7(b) shows the Tafel slope curves of the four samples in 0.5 mol L^{-1} H_2SO_4. It can be seen that the Tafel slopes of TiVCT$_x$, NF, TiVCT$_x$@NF and commercial platinum–carbon are 213 mV dec^{-1}, 180 mV dec^{-1}, 116 mV dec^{-1} and 29 mV dec^{-1}, respectively. The electrochemical test results show that the water splitting of the hybrid TiVCT$_x$@NF in the hydrogen evolution catalytic process is based on the Volmer–Heyrovsky reaction mechanism,[28] which involves the rapid hydrogen ion adsorption Volmer reaction ($H_3O^+ + e^- \rightarrow H_{ads} + H_2O$) and the slow hydrogen desorption Heyrovsky reaction ($H_{ads} + H_3O^+ + e^- \rightarrow H_2 + H_2O$). Previous

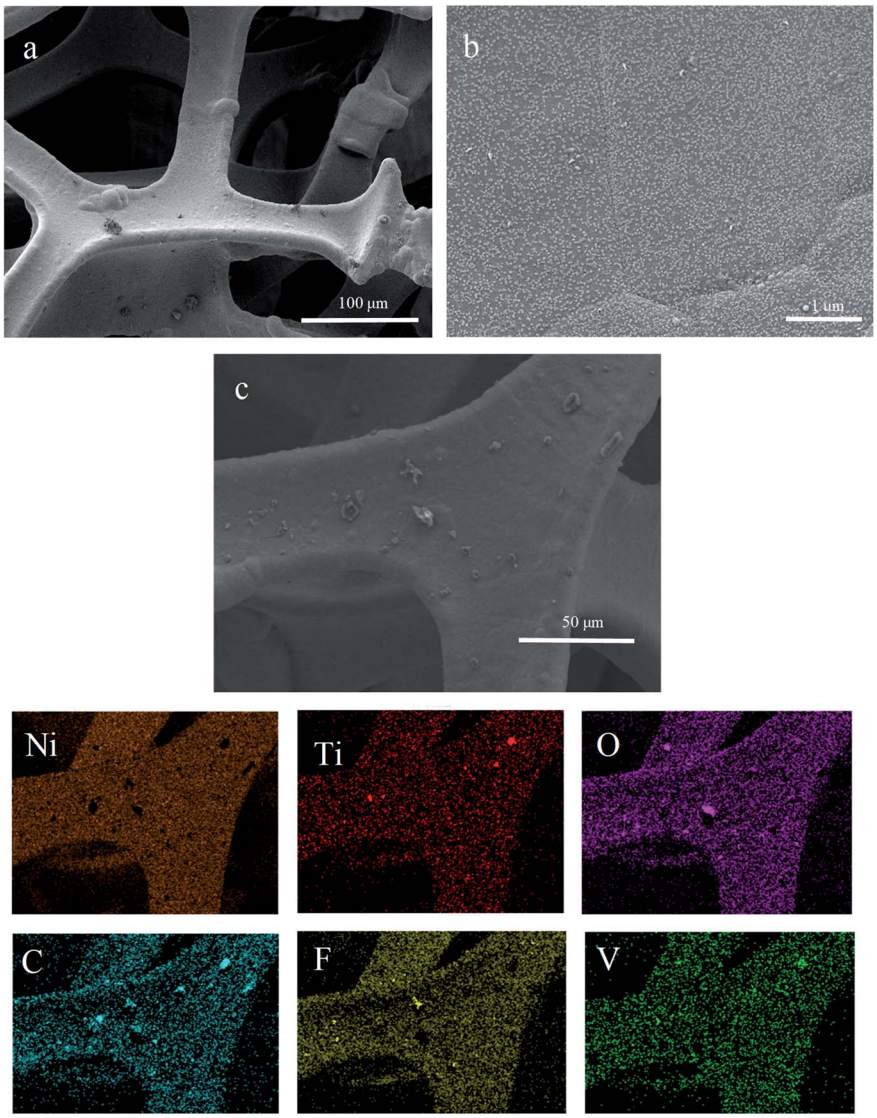

Fig. 4 (a and b) SEM images of TiVCT$_x$@NF. (c) Elemental mapping images of TiVCT$_x$@NF.

studies have shown that the active site of the HER is generally the –OH group, and the two basic steps of water splitting are as follows: (1) H_3O^+ ions are first adsorbed on the –OH group and then combined with electrons to generate a hydrogen atom. (2) The hydrogen atom generated in step 1 combines with an H_3O^+ ion and an electron to generate H_2. The hydrogen desorption process in step 2 is the rate-determining step of the hydrogen evolution catalytic reaction. In addition, other scholars have reported the excellent electrochemical performance of MXene electrodes, as shown in Fig. 7(c) and (d); with the same electrolyte conditions, the TiVCT$_x$@NF electrodes are superior to MXene electrodes ($Ti_3C_2T_x$,[29] RuS_A-$Ti_3C_2T_x$ (ref. 30) and $Mo_2TiC_2T_x$@NF[31]).

Furthermore, electrochemical impedance spectroscopy (EIS) was used to reveal the electron transfer kinetics of TiVCT$_x$@NF during the hydrogen evolution reaction. Fig. 8(a) presents a Nyquist plot of the four samples. In the Nyquist diagram, the impedance value represents the resistance encountered in the transfer of charges in the HER, and the smaller the arc radius, the smaller the impedance value of the test sample, indicating that the hydrogen evolution catalytic reaction is more likely to occur. The size of the semicircle is related to the electrode surface properties and determines the size of the charge transfer resistance (R_{ct}). It is obvious that the impedance value of the hybrid TiVCT$_x$@NF is significantly lower than that of the TiVCT$_x$ MXene. The electrochemical impedance spectrum is fitted using the Z-view software; the fitted resistance circuit diagram is shown in Fig. 8(b) and the related resistance parameter fitting results are presented in Table 1. R_1 represents the equivalent series resistance (ESR), which consists of three parts: the ionic resistance of the electrolyte, the resistance inside the active material and the current collector, and the interfacial contact resistance between the electrode and the electrolyte. R_2 represents the

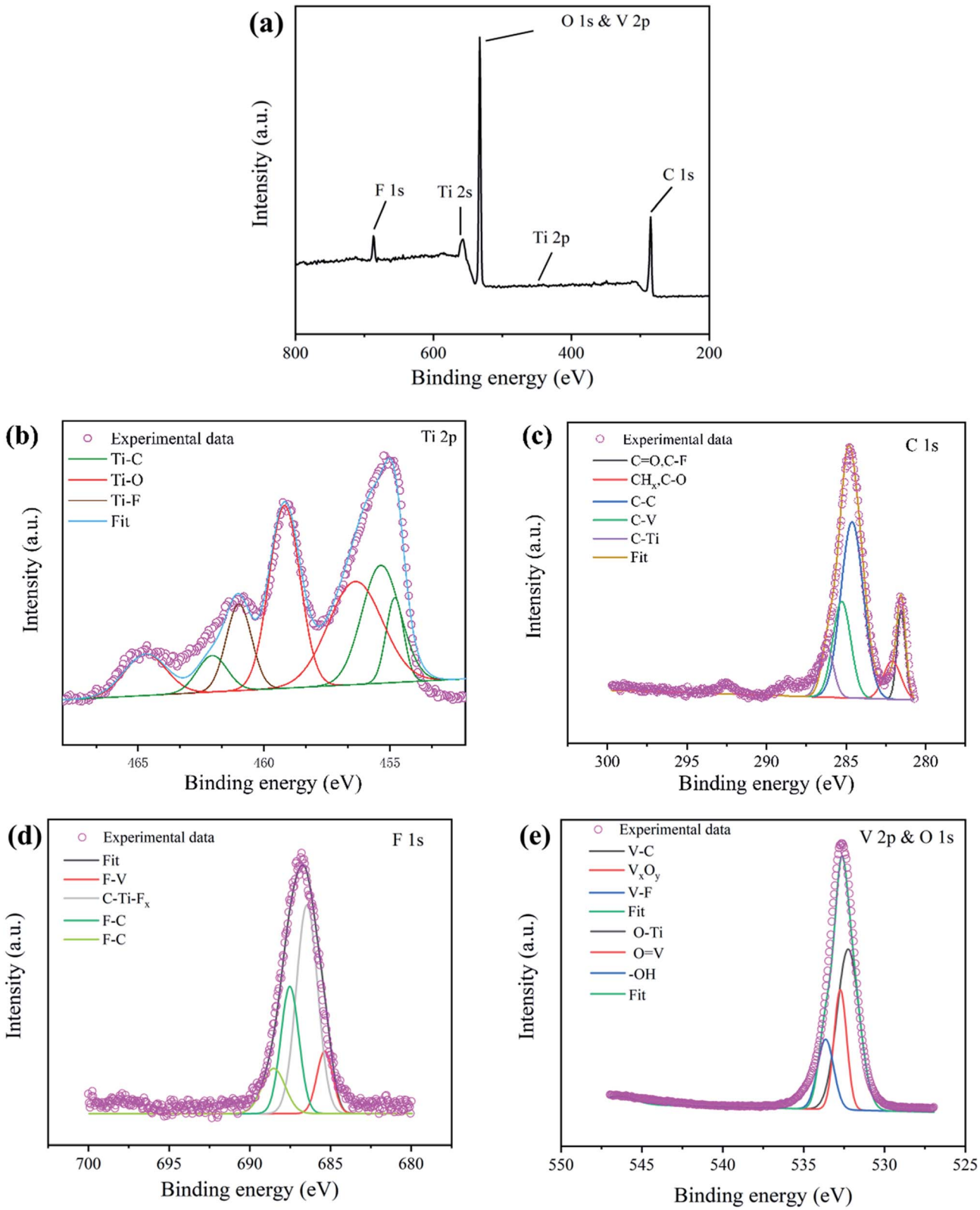

Fig. 5 XPS spectra of the TiVCT$_x$ MXene: (a) the full spectrum, (b) Ti 2p, (c) C 1s, (d) F 1s, (e) V 2p and O 1s.

diffusion resistance, which refers to the resistance caused by the transport of ions in a thin layer, which is related to the current changes, concentration changes, and electrode materials. R_3 represents the charge transfer resistance (R_{ct}). As shown in Table 1, the fitted resistance of TiVCT$_x$@NF is smaller than that of the other two electrode materials, and the

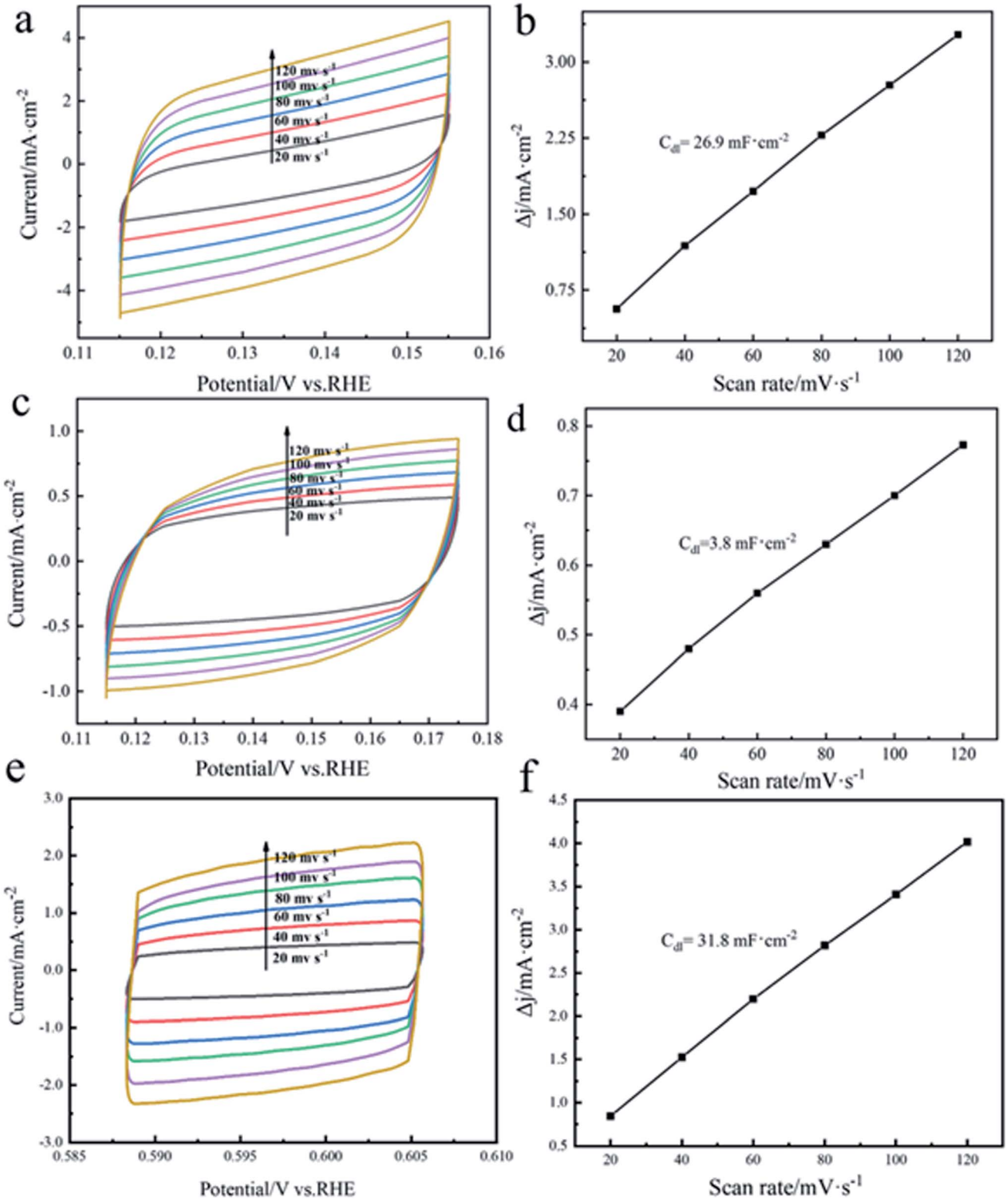

Fig. 6 Cyclic voltammetry curves of (a) TiVCT$_x$@NF, (c) TiVCT$_x$ and (e) commercial Pt/C recorded from −6 to 94 mV *vs.* RHE at scan rates of 20, 40, 60, 80, 100 and 120 mV s^{-1}. Estimated double-layer capacitances (C_{dl}) of (b) TiVCT$_x$@NF, (d) TiVCT$_x$ and (f) commercial Pt/C.

R_3 of TiVCT$_x$@NF is only 186.5 Ω. This indicates that the TiVCT$_x$@NF electrode system has a smaller internal resistance and larger electroactive surface, and it is easier for ions to penetrate between the sheets of the electrode material. These results indicate that TiVCT$_x$@NF has better electrochemical performance.

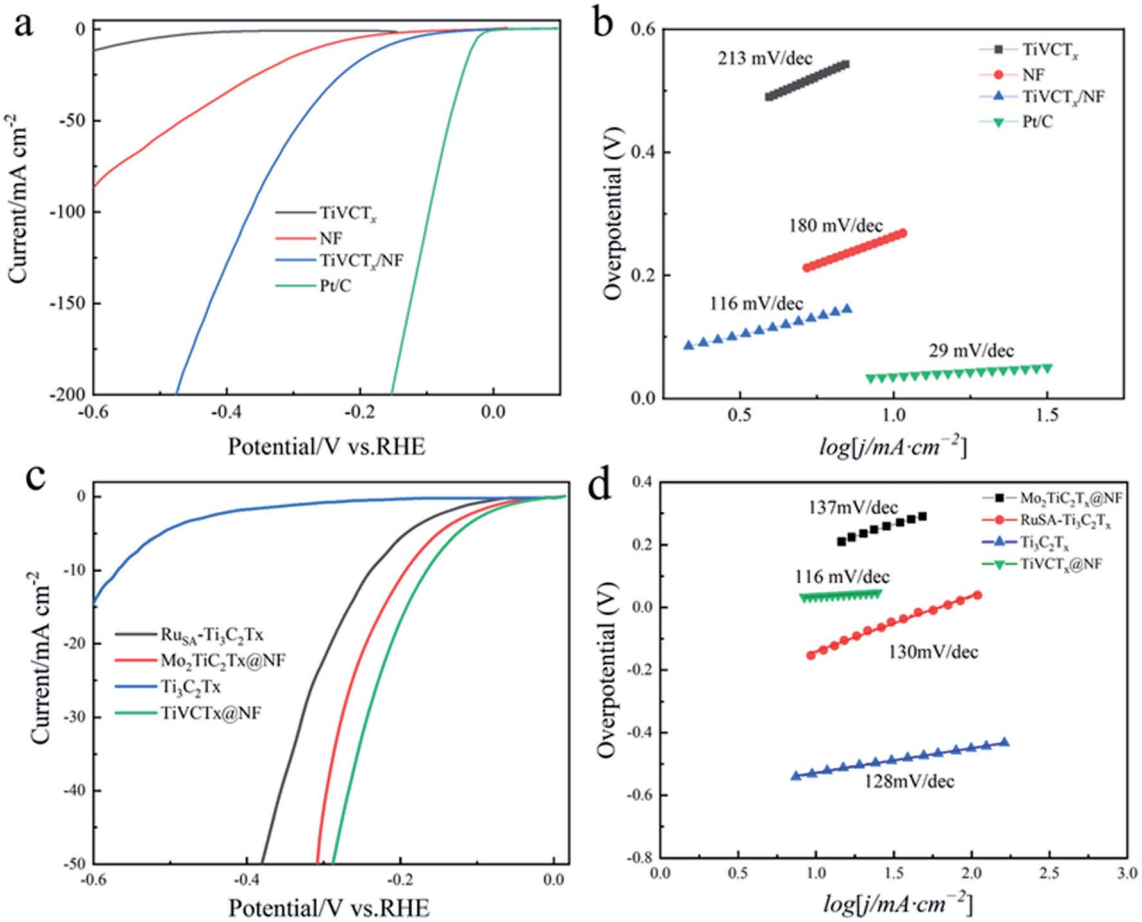

Fig. 7 (a) Polarization curves and (b) corresponding Tafel plots of $TiVCT_x$, $TiVCT_x$@NF, NF and commercial Pt/C at a scan rate of 10 mV s^{-1} in a 0.5 M H_2SO_4 solution. (c) Polarization curves and (d) corresponding Tafel plots of $Ti_3C_2T_x$, $TiVCT_x$@NF, RuS_A-$Ti_3C_2T_x$ and $Mo_2TiC_2T_x$@NF at a scan rate of 10 mV s^{-1} in a 0.5 M H_2SO_4 solution.

To evaluate the comprehensive performance of a hydrogen evolution catalyst, it is necessary not only to consider the catalytic activity of the hydrogen evolution reaction but also to test its stability. In order to examine the catalytic stability of the $TiVCT_x$@NF composites in 0.5 mol L^{-1} H_2SO_4, long-term CV cycling tests for 1000 cycles were carried out. As shown in Fig. 9(a), the time-dependent electrical density curve remains almost unchanged for the HER after 1000 test cycles. As shown

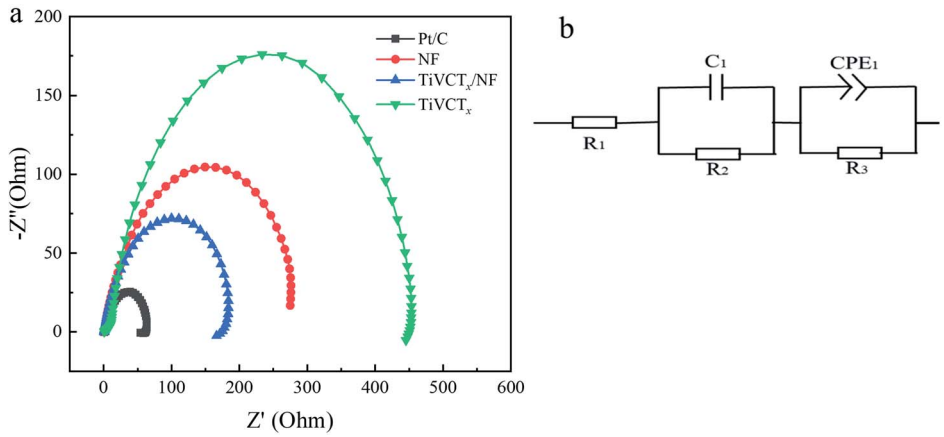

Fig. 8 (a) Electrochemical impedance spectra of Pt/C, NF, $TiVCT_x$ and $TiVCT_x$@NF for the electrocatalytic HER at an overpotential of open-circuit potential. (b) Equivalent circuit diagram of the $TiVCT_x$@NF composites.

Table 1 EIS fitting parameters of the $TiVCT_x$, NF and $TiVCT_x$@NF electrodes

Working electrode	R_1	R_2	R_3	C_1	CPE_1-T	CPE_2-T
$TiVCT_x$	15.62	115.1	2334	1.02×10^{-5}	6.39×10^{-6}	0.8533
NF	15.34	9.447	442.8	2.89×10^{-5}	5.17×10^{-6}	0.8693
$TiVCT_x$@NF	1.33	3.695	186.5	0.0079	0.0021	0.8247

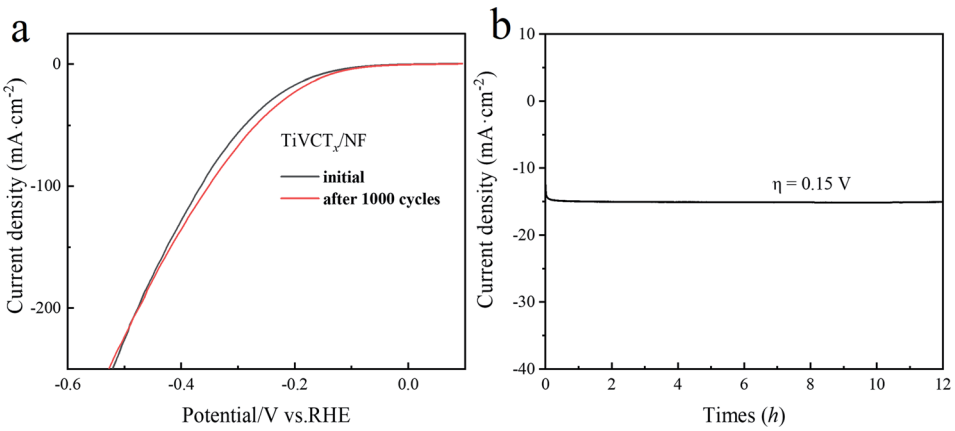

Fig. 9 (a) Polarization curves of $TiVCT_x$@NF initially and after 1000 CV cycles. (b) Current density *versus* time for $TiVCT_x$@NF at a 150 mV potential.

in Fig. 9(b), the catalytic activity for hydrogen evolution of $TiVCT_x$@NF remains almost unchanged at 0.15 V for 12 h. From the above results, it can be seen that the hybrid $TiVCT_x$@NF exhibits excellent HER catalytic activity and good stability during long-term electrolysis, indicating that $TiVCT_x$@NF is a highly stable electrocatalyst for HER.

4. Conclusion

In summary, $TiVCT_x$@NF was successfully prepared using the annealing method. Selecting a typical three-electrode system, the comprehensive electrochemical performance of $TiVCT_x$@NF was tested. The experimental results show that the composite $TiVCT_x$@NF exhibits excellent electrochemical properties with a low overpotential of 151 mV at 10 mA cm^{-2} and a small Tafel slope of 116 mV dec^{-1}. In a 0.5 M H_2SO_4 solution, $TiVCT_x$@NF exhibits excellent HER catalytic activity after 1000 test cycles and long-term stability over 12 h. Compared to the $TiVCT_x$ MXene, $TiVCT_x$@NF has more active sites and less resistance encountered in the transfer of charges in the HER. Based on these excellent electrochemical properties, $TiVCT_x$@NF is expected to be applied as an electrocatalytically active catalyst for water splitting.

Conflicts of interest

The authors declare no competing financial interest.

Acknowledgements

This work is financially supported by the Natural Science Foundation of China (51704221) and Outstanding Youth Science Foundation of Wuhan Polytechnic University (2018J05).

References

1 S. M. Fernández-Valverde, in *Hydrogen: The Ecological Fuel for Mexican Future*, Springer, 2007.
2 S. H. Jensen, P. H. Larsen and M. Mogensen, Hydrogen and synthetic fuel production from renewable energy sources, *Int. J. Hydrogen Energy*, 2007, **32**, 3253–3257.
3 M. G. Walter, E. L. Warren, J. R. McKone, S. W. Boettcher, Q. Mi, E. A. Santori and N. S. Lewis, Solar water splitting cells, *Chem. Rev.*, 2010, **110**, 6446–6473.
4 Y. Wei, R. A. Soomro, X. Xie and B. Xu, Design of efficient electrocatalysts for hydrogen evolution reaction based on 2D MXenes, *J. Energy Chem.*, 2021, **55**, 244–255.
5 Z. Li, Z. Qi, S. Wang, T. Ma, L. Zhou, Z. Wu, X. Luan, F. Lin, M. Chen and J. T. Miller, *In situ* formed Pt_3Ti nanoparticles on a two-dimensional transition metal carbide (MXene) used as efficient catalysts for hydrogen evolution reactions, *Nano Lett.*, 2019, **19**, 5102–5108.
6 H. Wang, Y. Wu, J. Zhang, G. Li, H. Huang, X. Zhang and Q. Jiang, Enhancement of the electrical properties of MXene Ti_3C_2 nanosheets by post-treatments of alkalization and calcination, *Mater. Lett.*, 2015, **160**, 537–540.
7 Z. Guo, L. Gao, Z. Xu, S. Teo, C. Zhang, Y. Kamata, S. Hayase and T. Ma, High electrical conductivity 2D MXene serves as

additive of perovskite for efficient solar cells, *Small*, 2018, **14**, 1802738.

8 Y. Zhang, X. Zha, K. Luo, Y. Qin, X. Bai, J. Xu, C. Lin, Q. Huang and S. Du, Theoretical study on the electrical and mechanical properties of MXene multilayer structures through strain regulation, *Chem. Phys. Lett.*, 2020, **760**, 137997.

9 Z. W. Seh, K. D. Fredrickson, B. Anasori, J. Kibsgaard, A. L. Strickler, M. R. Lukatskaya, Y. Gogotsi, T. F. Jaramillo and A. Vojvodic, Two-dimensional molybdenum carbide (MXene) as an efficient electrocatalyst for hydrogen evolution, *ACS Energy Lett.*, 2016, **1**, 589–594.

10 R. Tang, S. Xiong, D. Gong, Y. Deng, Y. Wang, L. Su, C. Ding, L. Yang and C. Liao, Ti_3C_2 2D MXene: recent progress and perspectives in photocatalysis, *ACS Appl. Mater. Interfaces*, 2020, **12**, 56663–56680.

11 L. Huang, L. Ai, M. Wang, J. Jiang and S. Wang, Hierarchical MoS_2 nanosheets integrated Ti_3C_2 MXenes for electrocatalytic hydrogen evolution, *Int. J. Hydrogen Energy*, 2019, **44**, 965–976.

12 T. A. Le, Q. V. Bui, N. Q. Tran, Y. Cho, Y. Hong, Y. Kawazoe and H. Lee, Synergistic effects of nitrogen doping on MXene for enhancement of hydrogen evolution reaction, *ACS Sustainable Chem. Eng.*, 2019, **7**, 16879–16888.

13 J. Liu, Y. Liu, D. Xu, Y. Zhu, W. Peng, Y. Li, F. Zhang and X. Fan, Hierarchical "nanoroll" like $MoS_2/Ti_3C_2T_x$ hybrid with high electrocatalytic hydrogen evolution activity, *Appl. Catal., B*, 2019, **241**, 89–94.

14 Z. He, T. Rong, Y. Li, J. Ma, Q. Li, F. Wu, Y. Wang and F. Wang, Two-Dimensional TiVC Solid-Solution MXene as Surface-Enhanced Raman Scattering Substrate, *ACS Nano*, 2022, **16**, 4072–4083.

15 S. Yazdanparast, S. Soltanmohammad, A. Fash-White, G. J. Tucker and G. L. Brennecka, Synthesis and surface chemistry of 2D TiVC solid-solution MXenes, *ACS Appl. Mater. Interfaces*, 2020, **12**, 20129–20137.

16 Y. Li, L. Li, R. Huang, Y. Zhang and Y. Wen, Computational screening of pristine and functionalized ordered TiVC MXenes as highly efficient anode materials for lithium-ion batteries, *Nanoscale*, 2021, **13**, 2995–3001.

17 Y. Li, J. Zhang, Y. Cheng, K. Feng, J. Li, L. Yang and S. Yin, Stable $TiVCT_x$/poly-*o*-phenylenediamine composites with three-dimensional tremella-like architecture for supercapacitor and Li-ion battery applications, *Chem. Eng. J.*, 2022, 134578.

18 J. R. McKone, B. F. Sadtler, C. A. Werlang, N. S. Lewis and H. B. Gray, Ni-Mo nanopowders for efficient electrochemical hydrogen evolution, *ACS Catal.*, 2013, **3**, 166–169.

19 G. Wang, J. Huang, S. Chen, Y. Gao and D. Cao, Preparation and supercapacitance of CuO nanosheet arrays grown on nickel foam, *J. Power Sources*, 2011, **196**, 5756–5760.

20 W. Kong, C. Lu, W. Zhang, J. Pu and Z. Wang, Homogeneous core-shell $NiCo_2S_4$ nanostructures supported on nickel foam for supercapacitors, *J. Mater. Chem. A*, 2015, **3**, 12452–12460.

21 T. Hussain, L. Truong, S. Hussain, S. A. Pital, S. Chun and M. Kaseem, Novel core-shell structured electrocatalyst with 1D-$NiTe_2$ over 3D metal structure for efficient hydrogen evolution reactions, *J. Alloys Compd.*, 2022, 165797.

22 T. Hussain, M. Hussain, S. Hussain and M. Kaseem, Microwave-assisted synthesis of $NiTe_2$ photocatalyst as a facile and scalable approach for energy-efficient photocatalysis and detoxification of harmful organic dyes, *Sep. Purif. Technol.*, 2022, **282**, 120025.

23 H. Zou, X. Li, C. Zhang, Y. Wen, Y. Fan, Y. Liu, L. Xiong, X. Zheng and J. Yang, Reactive synthesis for porous TiVAlC ceramics by TiH_2, V, Al and graphite powders, *Ceram. Int.*, 2021, **47**, 28288–28295.

24 S. Li, P. Tuo, J. Xie, X. Zhang, J. Xu, J. Bao, B. Pan and Y. Xie, Ultrathin MXene nanosheets with rich fluorine termination groups realizing efficient electrocatalytic hydrogen evolution, *Nano Energy*, 2018, **47**, 512–518.

25 X. Wang, J. Wang, J. Qin, X. Xie, R. Yang and M. Cao, Surface charge engineering for covalently assembling three-dimensional MXene network for all-climate sodium ion batteries, *ACS Appl. Mater. Interfaces*, 2020, **12**, 39181–39194.

26 P. Sharma and T. S. Bhatti, A review on electrochemical double-layer capacitors, *Energy Convers. Manage.*, 2010, **51**, 2901–2912.

27 S. A. Vilekar, I. Fishtik and R. Datta, Kinetics of the hydrogen electrode reaction, *J. Electrochem. Soc.*, 2010, **157**, B1040.

28 A. Lasia, Mechanism and kinetics of the hydrogen evolution reaction, *Int. J. Hydrogen Energy*, 2019, **44**, 19484–19518.

29 A. D. Handoko, K. D. Fredrickson, B. Anasori, K. W. Convey, L. R. Johnson, Y. Gogotsi, A. Vojvodic and Z. W. Seh, Tuning the basal plane functionalization of two-dimensional metal carbides (MXenes) to control hydrogen evolution activity, *ACS Appl. Energy Mater.*, 2017, **1**, 173–180.

30 V. Ramalingam, P. Varadhan, H. C. Fu, H. Kim, D. Zhang, S. Chen, L. Song, D. Ma, Y. Wang and H. N. Alshareef, Heteroatom-mediated interactions between ruthenium single atoms and an MXene support for efficient hydrogen evolution, *Adv. Mater.*, 2019, **31**, 1903841.

31 J. Wang, P. He, Y. Shen, L. Dai, Z. Li, Y. Wu and C. An, FeNi nanoparticles on Mo_2TiC_2Tx MXene@nickel foam as robust electrocatalysts for overall water splitting, *Nano Res.*, 2021, **14**, 3474–3481.